Showcasing research from Professor Huub de Groot's laboratory, Leiden Institute of Chemistry, Leiden University, Leiden, Netherlands.

An integrated approach towards extracting structural characteristics of chlorosomes from a *bchQ* mutant of *Chlorobaculum tepidum*

This image shows an integration of data recorded with MAS NMR (bottom right), cryo-EM (background), and circular dichroism spectroscopy (top left) in deducing the structure of *syn-anti* stacks within the chlorosomes of a mutant of *Chlorobaculum tepidum*. The visualization shows the orientation of the bacteriochlorophylls on the curved surface of a tubular assembly of molecular *syn-anti* stacks with a repeat of 1.49 nm in the direction of the tube axis that is highlighted with a yellow arrow.

As featured in:

ROYAL SOCIETY OF CHEMISTRY

rsc.li/pccp

PCCP Owner Societies

PCCP

Check for updates

An integrated approach towards extracting structural characteristics of chlorosomes from a *bchQ* mutant of *Chlorobaculum tepidum*†

Lolita Dsouza, [iD] [a] Xinmeng Li, [iD] [ab] Vesna Erić, [c] Annemarie Huijser, [iD] [d] Thomas L. C. Jansen, [iD] [c] Alfred R. Holzwarth, [iD] [e] Francesco Buda, [iD] [a] Donald A. Bryant, [iD] [f] Salima Bahri, [iD] [g] Karthick Babu Sai Sankar Gupta, [iD] [a] G. J. Agur Sevink [iD] *[a] and Huub J. M. de Groot [iD] *[a]

Chlorosomes, the photosynthetic antenna complexes of green sulfur bacteria, are paradigms for light-harvesting elements in artificial designs, owing to their efficient energy transfer without protein participation. We combined magic angle spinning (MAS) NMR, optical spectroscopy and cryogenic electron microscopy (cryo-EM) to characterize the structure of chlorosomes from a *bchQ* mutant of *Chlorobaculum tepidum*. The chlorosomes of this mutant have a more uniform composition of bacteriochlorophyll (BChl) with a predominant homolog, [8Ethyl, 12Ethyl] BChl *c*, compared to the wild type (WT). Nearly complete ^{13}C chemical shift assignments were obtained from well-resolved homonuclear ^{13}C–^{13}C RFDR data. For proton assignments heteronuclear ^{13}C–^{1}H (hCH) data sets were collected at 1.2 GHz spinning at 60 kHz. The CHHC experiments revealed intermolecular correlations between $13^2/3^1$, $13^2/3^2$, and $12^1/3^1$, with distance constraints of less than 5 Å. These constraints indicate the *syn*–*anti* parallel stacking motif for the aggregates. Fourier transform cryo-EM data reveal an axial repeat of 1.49 nm for the helical tubular aggregates, perpendicular to the inter-tube separation of 2.1 nm. This axial repeat is different from WT and is in line with BChl *syn*–*anti* stacks running essentially parallel to the tube axis. Such a packing mode is in agreement with the signature of the Q_y band in circular dichroism (CD). Combining the experimental data with computational insight suggests that the packing for the light-harvesting function is similar between WT and *bchQ*, while the chirality within the chlorosomes is modestly but detectably affected by the reduced compositional heterogeneity in *bchQ*.

1. Introduction

Green sulfur bacteria are nonmotile, Gram-negative bacteria that thrive in strictly anaerobic environments. They are predominantly found in hot springs, sediments, and mats, and in stratified aquatic environments.[1–3] The unique feature of these bacteria is that they can survive in extremely low light environments and can harvest light very efficiently.[4,5] The ability of these bacteria to survive in low light and efficiently transfer energy is due to their use of efficient chlorosome antenna structures.[6,7]

Chlorosomes harvest light and subsequently transfer the excitation energy to the baseplate, then to the FMO bacteriochlorophyll (BChl) *a*-binding protein, and ultimately to the reaction center facilitating charge separation.[8–11] The self-assembly of chlorosomes is due to aggregates of BChls that form without involving proteins.[8,12] The distinctiveness of BChl *c*, the major pigment in chlorosomes, lies in its 3^1 hydroxyl group and the absence of a methyl carboxyl group at the 13^1 position, see Fig. 1. The limited bulkiness of the functionalities at the 3^1 and 13^1 positions enables the formation of large supramolecular aggregates by favorable modulation of steric hindrance.[13] Self-assembly is a thermodynamically favorable

[a] Leiden Institute of Chemistry, Leiden University, Einsteinweg 55, 2300 RA, Leiden, The Netherlands. E-mail: ssnmr@chem.leidenuniv.nl

[b] Department of Chemistry and Hylleraas Centre for Quantum Molecular Sciences, University of Oslo, 0315, Oslo, Norway

[c] Zernike Institute of Advanced Materials, University of Groningen, Nijenborgh 4, 9747 AG, The Netherlands
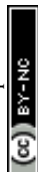
[d] MESA+ Institute for Nanotechnology, University of Twente, 7500 AE, The Netherlands

[e] Max Planck Institute for Chemical Energy Conversion, Stiftstraße 34-36, 45470, Mülheim an der Ruhr, Germany

[f] Department for Biochemistry and Molecular Biology, The Pennsylvania State University, University Park, Pennsylvania 16802, USA

[g] NMR Spectroscopy, Bijvoet center for Biomolecular Research, Utrecht University, Padualaan 8, 3584 CH, Utrecht, The Netherlands

† Electronic supplementary information (ESI) available. See DOI: https://doi.org/10.1039/d4cp00221k

15856 | *Phys. Chem. Chem. Phys.*, 2024, **26**, 15856–15867

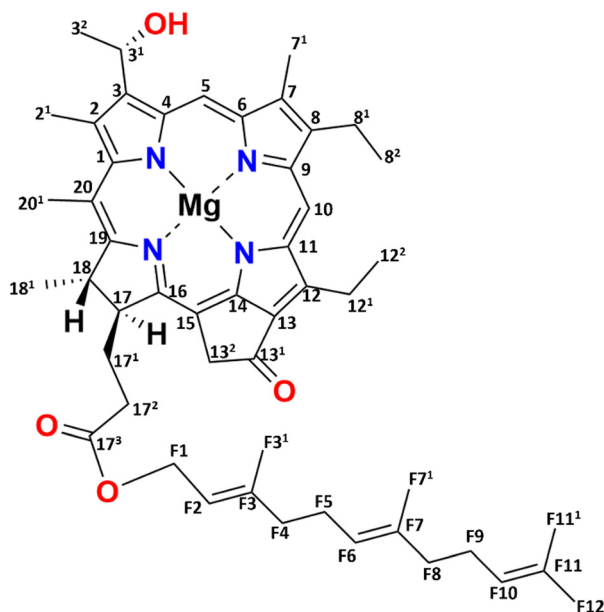This journal is © the Owner Societies 2024

Fig. 1 Chemical structure of [8Et, 12Et] BChl *c*, which is the most abundant (95%) BChl *c* homolog for the *bchQ* mutant of *Chlorobaculum tepidum*.

process and for chlorosomes, it is enabled by four main types of intermolecular interactions, (i) coordination of the central magnesium ion to the hydroxyl group, (ii) hydrogen bond formation between the carbonyl group and the hydroxyl group, (iii) pi–pi stacking of the chromophores and (iv) hydrophobic interactions of the tails.[14,15] Hydrogen bonding was previously considered to play a dominant role in the emergence of two spectral components.[16] With a major component consisting of hydrogen bond donors that support Mg–OH$\cdots$O=C motifs connecting BChls within and between *syn–anti* stacks, and a minor fraction for which the Mg–OH coordination between BChls in a stack is present, H-bonds between stacks cannot be formed due to the partial rotation of BChls in the plane of their macrocycle.[16] The BChls of the second fraction were therefore regarded as non-donors for hydrogen bonds.[17] The presence of two fractions agrees with the observed dispersion of the optical absorption profile and the splitting of the NMR signals.[14,17,18] The aliphatic functionalities at the 8 and 12 positions are thought to assist in optimizing the size of the BChls and produce steric hindrance for tuning their absorption properties. They provide an overall broadening of the optical absorption profile by side chain heterogeneity.[13]

One chlorosome organelle can contain up to several hundred thousand BChl pigments. Although every chlorosome is unique in both size and composition, for the *bchQ* mutant they are 95–163 nm in length and 31–57 nm in diameter on average.[5,19] Structuring BChl molecules in chlorosomes is a natural solution to overcome the rapid loss of excitonic energy that otherwise would occur for this high pigment density. Naturally self-assembled BChl aggregates like chlorosomes thus provide a paradigm for the bottom–up chemical engineering of biomimetic dye materials for use in optoelectronic

devices.[20,21] Significant advancements have been made in the analysis of the BChl biosynthesis pathway, leading to the construction of numerous mutations affecting BChl *c/d/e*.[13,22] Inactivation of CT1777, also known as *bchQ*, causes the accumulation of 5% [8Et, 12Me] and 95% [8Et, 12Et]-BChl *c* homologs, see Fig. 1, unlike WT chlorosomes, that are comprised of four homologs: 5% [Et, Me], 60% [Et, Et], 30% [Pr, Et] and 5% [Bu, Et].[23] Because the homolog [8Et, 12Et] is also the major component in WT chlorosomes, it was taken as the representative pigment component in recent physical modelling studies.[16,17,20,24,25]

In this paper, we have combined three different methods to study the structural and optical characteristics of chlorosomes of the *bchQ* mutant of *Cba. tepidum*. While the side chain variability at the 8 and 12 positions is not anticipated to play a significant role, it is known to tune structural features and absorption properties.[23] Because of its nearly homogeneous composition, chlorosomes of the *bchQ* mutant are being studied experimentally in the present work. The use of mutants and the integration of different techniques has been a successful approach in determining the structure of chlorosomes in *Cba. tepdium*.[26–29] Following Ganapathy *et al.*, we combine two methods, solid-state magic angle spinning (MAS) nuclear magnetic resonance (NMR) spectroscopy and cryo-EM, to first resolve important structural features of BChl *c* packing in *bchQ* chlorosomes.[26] Additionally, we performed optical measurements. The obtained data were subsequently discussed in relation to earlier findings of WT chlorosomes and employed to propose a chiral angle for *bchQ*. In addition to the structure and optical properties, we used the dynamic spectral editing technique (DYSE) with solid-state NMR to study the dynamics between WT and *bchQ*.

2. Materials and methods

2.1. Sample preparation

The cells for *bchQ* and WT were grown at 40 °C in a growth chamber according to standard procedures.[1] For uniform ^{13}C labeling, 1.0 L of the Wahlund medium was inoculated with 50 mL freshly grown cell culture without ammonium acetate and grown for 1 day for light adaptation. 1.0 L of the fresh medium containing 99.5% enriched NaH^{13}CO$_3$ was inoculated with 50 mL of light-adapted culture grown without ammonium acetate.[15] Cells were grown for 2 days, then harvested at 12 000 × *g* by centrifugation. The supernatant was discarded, and the pellet was resuspended in 35 mL of 20 mM Tris-HCl (pH 8.0), 10 mM sodium ascorbate, and 2 M sodium thiocyanate. The pellet was completely dissolved by keeping it at 4 °C for 30 minutes. The cells were disrupted using a French pressure cell at 8.27 MPa at 4 °C. Then, 1.5 mg of DNAse-1 was added to the suspension and stirred for 30 minutes. The cells were passed through the French pressure cell again to ensure complete disruption. The suspension was centrifuged for 20 minutes at 23 200 × *g* to remove large cell debris in a Beckman ultra-centrifuge using a Ti-70 rotor. After centrifugation, the

This journal is © the Owner Societies 2024

Phys. Chem. Chem. Phys., 2024, **26**, 15856–15867 | **15857**

chlorosomes were isolated by subjecting them to centrifugation on a linear 20–50% sucrose density gradient. The separation process was carried out by subjecting the mixture to sucrose density gradient centrifugation in a swing-out rotor at 4 °C for 18 h at 133 668 × g. The sample was dialyzed overnight against 20 mM Tris-HCl buffer to remove sucrose and cyanate.[30] After dialysis, the optical absorption profile was collected using UV-Vis measurement. The sample was stored at 4 °C until further use. For solid-state NMR studies, the sample was further concentrated using an ultracentrifuge at 200 000 × g for 1 hour, and the obtained pellet was used to fill the NMR rotor in the form of a paste.

2.2. Solid-state NMR measurements

Central to this work is the use of MAS NMR, which has been developed over five decades into a versatile tool for studying biological systems, starting with the pioneering work on bacteriorhodopsin by Herzfeld *et al.*[31]

MAS-NMR data were collected from freshly prepared ^{13}C-labeled chlorosomes from *bchQ* and WT cells. The measurements were performed with the sample in a 3.2 mm rotor spinning at 11 kHz at the magic angle in a Bruker AV-750 (17.6 T) spectrometer equipped with a triple resonance MAS probe head by using a ^{13}C radio frequency of 188.6 MHz. One-dimensional, direct polarization (DP), cross polarization (CP) and insensitive nuclei enhanced by polarization transfer (INEPT) measurements were performed with 1024 scans.[32] The recycle delay was set to 2 s for CP and the delay period was set to 1.75 ms and 1.15 ms for INEPT. The proton π/2 pulse length for the CP was 2.5 μs, corresponding to 100 kHz rf amplitude. Two-dimensional dipolar correlation spectra were recorded by using ^{13}C–^{13}C radiofrequency driven recoupling (RFDR) at mixing times of 9.2 ms and 3.2 ms to probe long and short-range correlations.[33] The NMR data were collected in 256 scans for every trace in the t_1 dimension with phase-sensitive detection in ω_1. Two-dimensional dipolar correlation spectra were recorded by using the ^{13}C–^{13}C CHHC/CP[3] sequence to probe the indirect detection of ^{1}H–^{1}H contacts at proton diffusion times of 350 μs.[34,35] The dipolar hCH spectra were collected with a 1.3 mm probe in a 1.2 GHz spectrometer operating at a magnetic field strength of 28.2 Tesla. The sample was spun at 60 kHz at a set temperature of 245 K, which corresponds to a sample temperature of 277 K.[36] To assign the proton chemical shifts we made use of ^{13}C chemical shifts. The ^{1}H chemical shift was internally calibrated using the water signal at 4.7 ppm. In the 2D dipolar hCH spectra, 90° pulses were set at 105 kHz rf-field amplitude for ^{1}H and at 51 kHz rf-field amplitude for ^{13}C.[37,38] ^{1}H–^{13}C forward cross-polarization (CP) was achieved using a contact time of 1.2 ms. ^{13}C–^{1}H back CP was achieved using a contact time of 0.3 ms, and PISSARRO decoupling was used for both ^{1}H and ^{13}C with 15 kHz RF amplitude.[39] The MISSISSIPPI water suppression was used to suppress the water signal, with a 17 kHz irradiation for 120 ms.[40] All the spectra were acquired and processed using the states-TPPI procedure. See ESI† Table S4 for more information on the set up of solid state 2D NMR.

The data were processed using a Bruker TopSpin 4.1.4 and analyzed using MestReNova.

2.3. cryo-EM measurements

cryo-EM was performed with a Titan Krios microscope (FEI). Aliquots of purified chlorosomes were applied onto a holey carbon grid with a thin layer of carbon and were plunge frozen in liquid ethane at 83 K with a Vitrobot vitrification system (FEI). Experiments were performed with a Falcon 3 camera operated in a linear mode with a defocus of −0.5 μm. A magnification of 75 000 was used which corresponds to a pixel size of 0.878 Å per pixel. The image processing and analysis was performed using Fiji software.[41]

2.4. Optical measurements

UV-Vis spectra were measured using a Shimadzu 1800 UV-Vis spectrometer, with the sample contained in a 1 mm optical path length micro cuvette (Hellma, QS absorption cuvette). CD spectra were measured using a JASCO J-815 CD spectrometer, with the sample contained in a 1 mm optical path length micro cuvette (Hellma, QS absorption cuvette).

2.5. cryo-EM mimics

A pre-assembled BChl *c* tube structure with a helical angle of δ = 90° was taken from our previous set of structures.[20] The tube structure was 15 nm in diameter and 60 nm in length and was thermalised through 10 ns of molecular dynamics (MD) simulations. Using the EMAN2 package, we generated 6 Å resolution electron density maps (e2pdb2mrc.py) and obtained 2D projections (e2project3d.py). We performed Fourier Transform analysis over the 2D density maps using the Fiji software.[41]

3. Results

3.1. Structure of chlorosomes of *bchQ* based on MAS NMR and cryo-EM

The ^{13}C NMR chemical shift assignments for the BChl *c* molecules in the chlorosomes of the *bchQ* mutant of *Cba. tepidum* were obtained from 2D ^{13}C–^{13}C magic angle dipolar correlation spectra. Assignments are summarized in the ESI,† Table S1. Fig. 2 is an RFDR homonuclear dipolar correlation dataset collected with a mixing time of 9.2 ms. The measurements were also done at 3.2 ms which is used to predict the short-range correlations, shown in Fig. S4, in the ESI.† While the assignments closely match the assignments of the WT, the resonances were better resolved for the chlorosomes of the *bchQ* mutant. Like WT chlorosomes, a doubling of signals is observed for the mutant, for ^{13}C resonances 2^1-C, 3^1-C, 3^2-C, 4-C, 5-C, 6-C, 7-C, and 7^1-C of the BChl ring, revealing two different BChl components within the system.[16,17] The ^{13}C chemical shifts were used to calculate the aggregation shifts (see the ESI† Fig. S3). The BChl aggregates tend to shift upfield or downfield relative to monomeric BChl in solution due to the macrocycle overlap between neighboring BChl molecules that
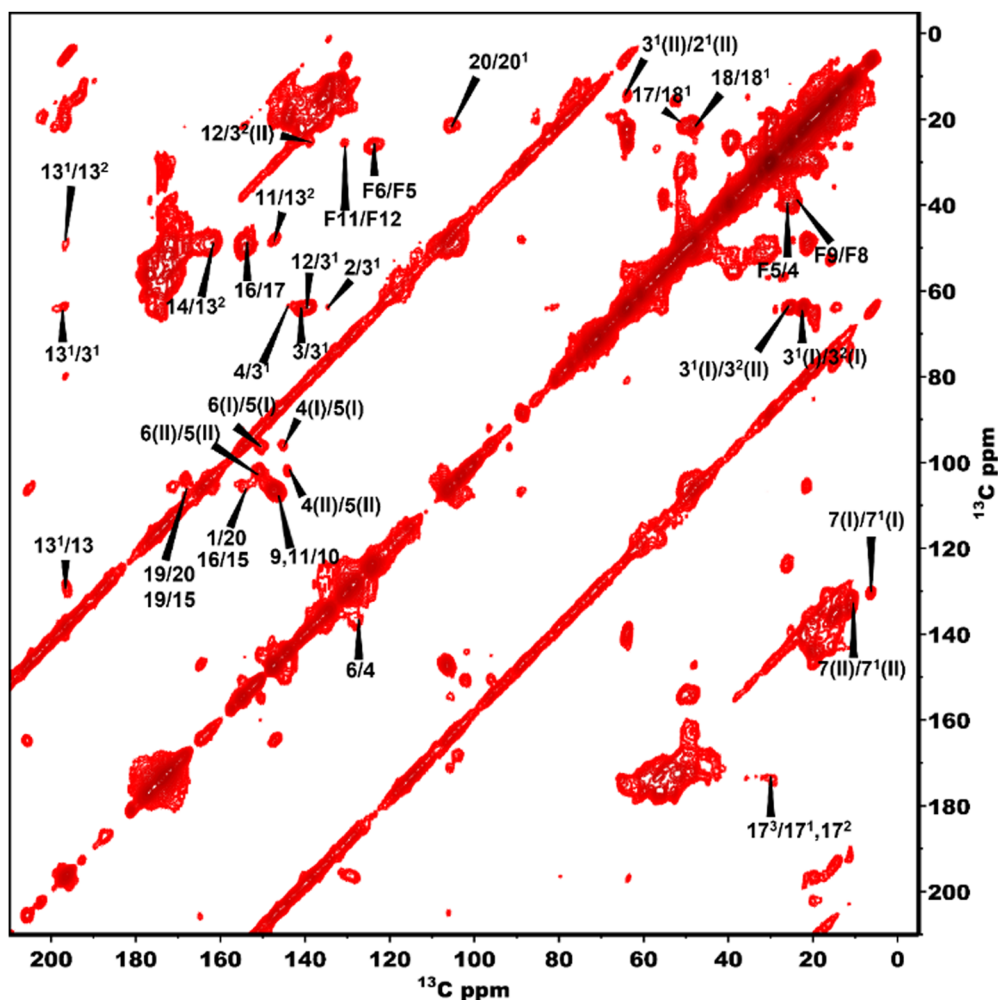
15858 | *Phys. Chem. Chem. Phys.*, 2024, **26**, 15856–15867

This journal is © the Owner Societies 2024

Fig. 2 ^{13}C–^{13}C RFDR spectra of *bchQ* with assignments recorded at 277 K, 11 kHz, 9.2 ms mixing time.

can give rise to significant ring current shifts.[21,42] The solution data for the ^{13}C were taken for the [8Et, 12Et] homolog as it is the most abundant homolog in the *bchQ* mutant.[15] The 2^1, 3, 3^2, 5, 7, 7^1, 8^2, 12, 12^1, 12^2, 19 and F3 carbons are shifted by $>|1.5|$ ppm or more relative to the data for monomeric BChl *c* in solution.

Fig. 3 shows a 2D dipolar hCH spectrum obtained at 60 kHz spinning frequency under a 28.2 Tesla magnetic field which gives rise to well-resolved cross peaks. The specific aim of this experiment is to resolve the ^{1}H shifts correlating with ^{13}C for the chlorosomes of the *bchQ* mutant. Protons have a high gyromagnetic ratio and are abundant spins.

Due to strong homonuclear dipolar couplings and little shift dispersion for ^{1}H, it is not easy to obtain well-resolved spectra.

To overcome this problem, the use of a high magnetic field in combination with faster spinning and inverse detection is beneficial.[43] Proton assignments are provided in Table S2 in the ESI.† The doubling for 5 and 7^1 that is observed for ^{13}C is also seen for protons. Upfield shifts >-1.5 ppm are detected for 2^1(I and II), 3^1, 5 (I and II), 7^1, 8^1, 12^1, and downfield shifts >1.5 ppm for 18^1 proton resonances compared to BChl *c* in solution.[14] The ^{1}H chemical shifts were used to calculate the

aggregation shifts (see the ESI,† Fig. S3). To proceed from chemical shift assignments and aggregation shift calculations to distance constraints, we collected homonuclear ^{13}C–^{13}C dipolar correlation data for the *bchQ* mutant, which gave us three unambiguous intermolecular correlations, namely $13^2/3^1$, $13^2/3^2$ and $12^1/3^1$, correlating carbons from ring 1 and ring 3 (Fig. 4).

cryo-EM observations reveal that *bchQ* chlorosomes are tubular in nature and are similar to WT chlorosomes.[27] A side-on view of isolated chlorosomes shows striped patterns, Fig. 5(a), which, after fast Fourier transform (FFT) of the image, yielded layer lines indicative of helicity/chirality of the pigment stacking within tubes, with an axial repeat of 1.49 nm, Fig. 5(b). The strongest pair of equatorial reflections relate to a 2.1 nm inter-tube distance. While the latter is in complete agreement with the WT case and pertains to the presence of the same aliphatic tail in the BChl pigment, the axial repeat of *bchQ* is significantly increased compared to the 1.25 nm for WT. This points to a difference in the chiral angle between *bchQ* and WT.

3.2. Optical characteristics of the chlorosomes

Optical responses, such as UV-Vis absorption and circular dichroism (CD), have been measured for chlorosomes of both
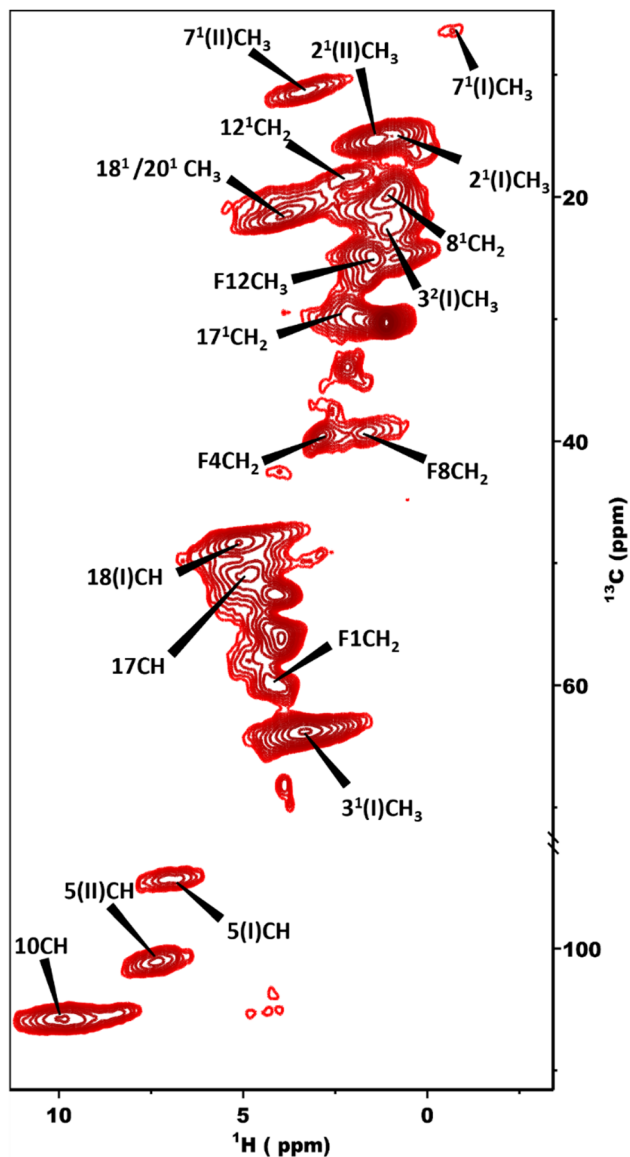
Fig. 3 2D dipolar hCH spectrum obtained at 1.2 GHz with the sample in a 1.3 mm rotor spinning at 60 kHz at a sample temperature of 277 K.

Fig. 4 (a) ^{13}C–^{13}C CHHC spectra of chlorosomes of *bchQ* recorded in a field of 17.6 T using an 11 kHz spinning frequency at 277 K. A ^{1}H–^{1}H spin diffusion mixing time of 350 μs was used. Intermolecular correlations are labelled in blue. (b) Intermolecular correlations between protons for the *syn–anti* parallel stacking arrangement, showing the shortest distances between protons of the correlating carbons. The stacking is in the vertical direction, with *syn*-BChl *c* shown in purple and *anti*-BChl *c* in yellow. Blue, green, orange, and red colouring schemes were used to indicate the 12^2, 3^1, 13^2, and 3^2 positions, respectively, which yielded cross peaks.

WT and *bchQ*. For WT chlorosomes, absorption, linear dichroism and CD spectra have been collected before from preparations with variable heterogeneity and homolog composition.[8] In particular the CD appears to depend strongly on the composition. We therefore performed independent measurements for the WT chlorosomes grown in well-controlled high light conditions and found the measured spectra to reproduce well between preparations.

Chlorosomes are quasi one-dimensional, and due to the *syn–anti* parallel stacking of the BChl *c* molecules there are both positive and negative couplings.[44] As a result, the Q_y absorbance bands of BChl *c* were observed at 750 nm for the WT and 735 nm for the *bchQ*. The overall shift towards longer wavelength in both WT and *bchQ* in comparison to monomeric BChl *c* in solution originates from strong excitonic coupling that leads to excitonic delocalization.[11,17]
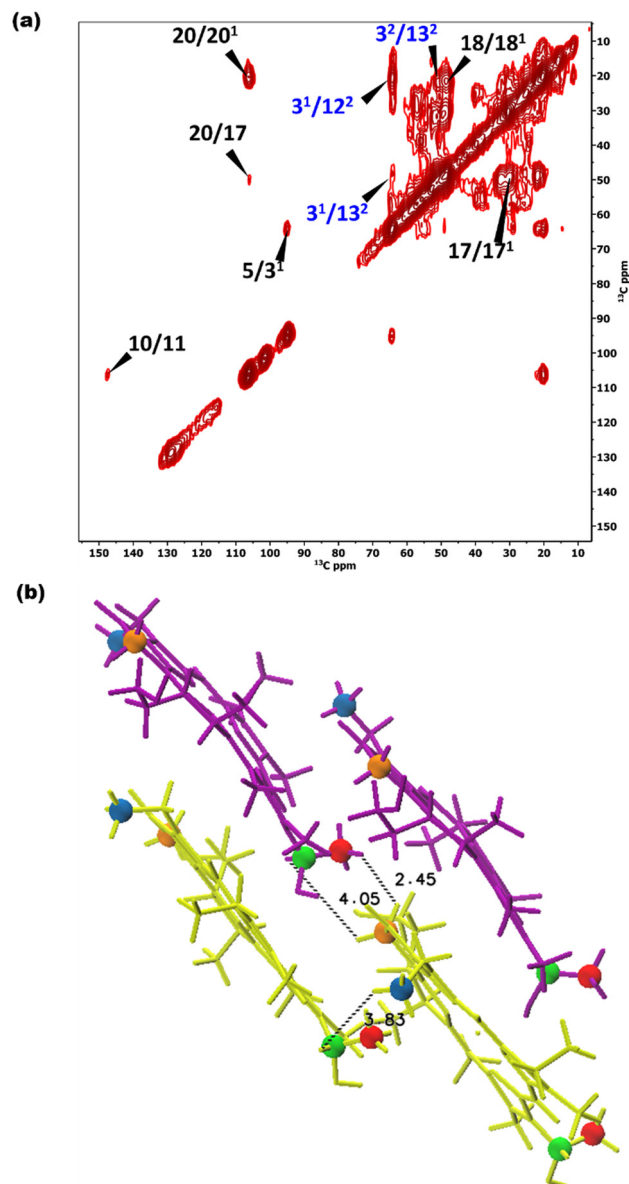
Among UV and CD, it has been reported that CD is sensitive to chirality.[20,24,45] We find psi shaped bands featuring a negative/positive/negative (−/+/−) signature in the CD spectra of both chlorosomes. Yet, the details clearly show a difference: for instance, the very intense negative band in the 750–800 region for the WT is almost absent for *bchQ*. In addition to this, the bands for *bchQ* are shifted in absolute terms and have different rotational strengths relative to WT (Fig. 6).
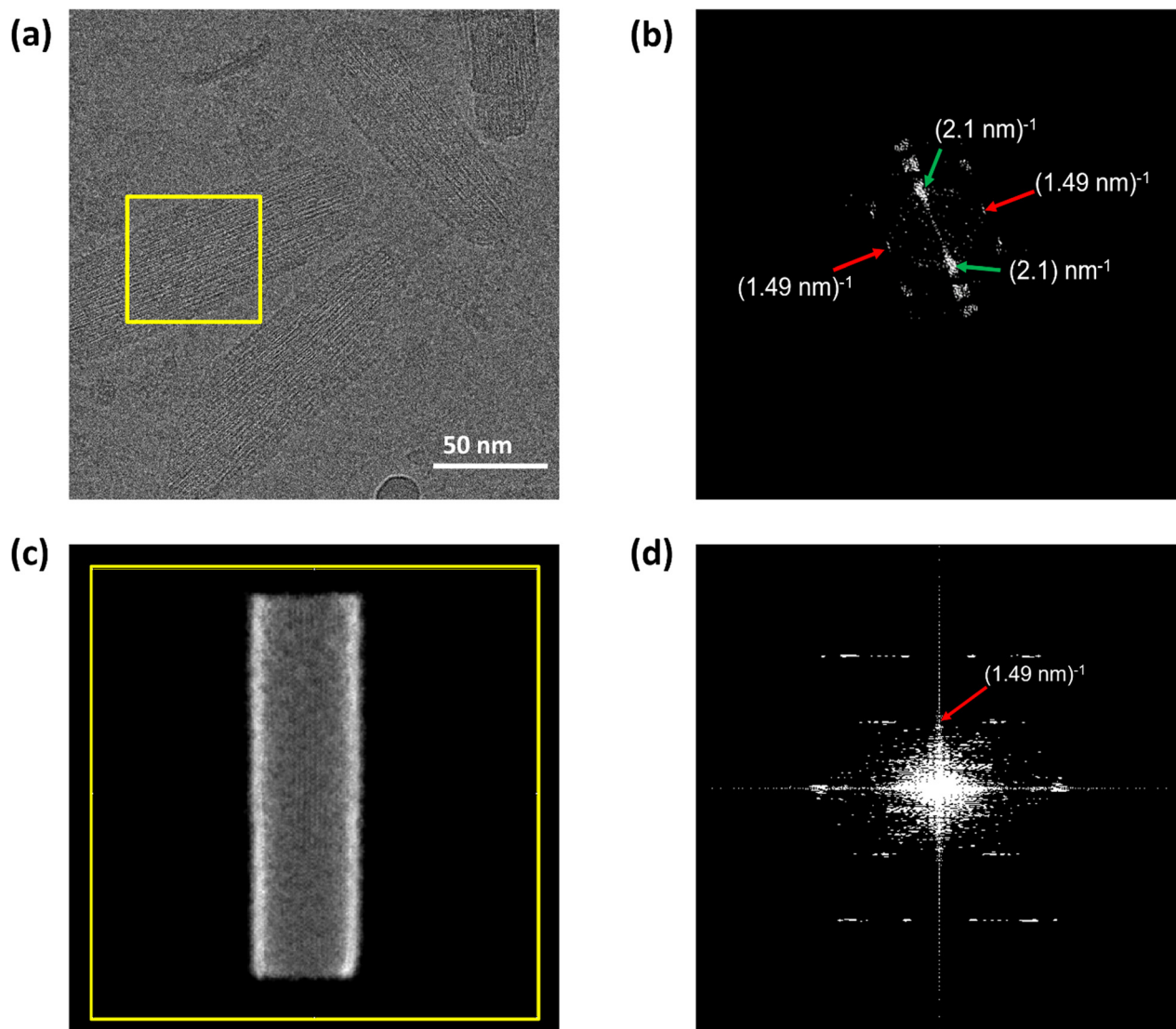
Fig. 5 Cryo-EM image of chlorosomes of the *bchQ* mutant of *Cba. tepidum* embedded in amorphous ice. (a) Is the side view, (b) shows the Fourier transform of the yellow boxed region in figure (a). The green arrows indicate reflections originating from a 2.1 nm spacing between BChl tubes and the red arrow indicates a layer line at a reciprocal distance of 1.49 nm. (c) Shows the projected simulated electron density corresponding to an atomistic model of a tube, of 15 nm in diameter and 60 nm in length constructed for a chiral angle $\delta = 90°$ and (d) is the Fourier transform of the projected electron density in (c). Both the position and structure of the layer line corresponding to the model system are in good agreement with the experimental layer line.

From the absorption spectra, one may identify a clear 15 nm red shift in the absorption maxima of chlorosomes of WT compared to the *bchQ* mutant, from 750 nm for the WT to 735 nm for the *bchQ* mutant. It has been noted that a small change in the absorption maxima from 750 nm to a lower wavelength can result in the attenuation of the longest wavelength negative band while strengthening the band at 720 nm.[46] In the current context, it is noticeable that the absorption maximum of *bchQ* chlorosomes is at approximately 735 nm, whereas it is around 750 nm in WT chlorosomes.

3.3. Structural dynamics of *bchQ* chlorosomes in comparison to WT

To also study the structural dynamics features in our sample, we employed a dynamic spectral editing (DYSE) approach.

We performed three distinct types of experiments: direct polarization (DP), cross polarization (CP) and Insensitive nucleus enhanced by polarization transfer (INEPT).[32] DP provides all the ^{13}C signals present in the sample, and it is only moderately affected by mobility in the system whereas CP and INEPT act as dynamic filters. CP probes motion around the millisecond time scale and is most effective if the system is rigid.[47] When there is significant isotropic motion in the system, dipolar couplings are averaged to zero, making CP inefficient, resulting in CP acting as a dynamic filter to probe rigid parts of the system. On the other hand, INEPT is effective only if the coherence lifetimes (T2) of carbons are long. Because this is not the case for rigid solids, INEPT selectively probes dynamic phenomena within the system.[32,48]

Fig. 7(a) shows a comparison of the INEPT spectra, highlighting the flexible domains in the system for the *bchQ* (red)

This journal is © the Owner Societies 2024

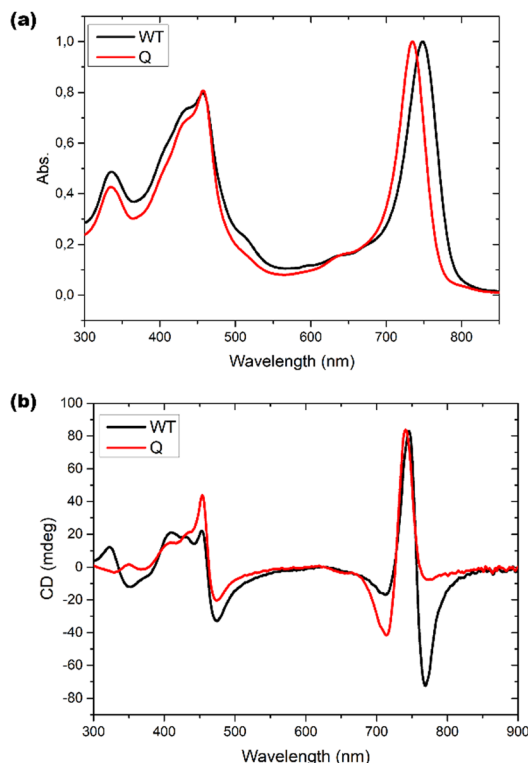*Phys. Chem. Chem. Phys.*, 2024, **26**, 15856–15867 | **15861**

Fig. 6 (a) UV-Vis absorption spectra and (b) CD spectra for WT (black) and *bchQ* (red), respectively, measured at room temperature.

and WT (black) chlorosomes. The spectra for the *bchQ* chlorosomes show increased signal intensity from galactolipids that resonate between 65–80 ppm and at 100 ppm. Each BChl contains fifty carbon atoms, out of which sixteen are quaternary carbons. Quaternary carbons which resonate above 130 ppm do not show any signal in the INEPT. The signals originating from the tail ^{13}C resonances are F1-CH$_2$, F4-CH$_2$, F5-CH$_2$, F10-CH, F3^1-CH$_3$, and side chains 17-CH, 18-CH, 17^1-CH$_2$, 17^2-CH$_2$, 3^2-C, 2^1-C, 7^1-C, 8^1-C, 8^2-CH$_3$. The table with the position and chemical shifts is given in the ESI,† Table S3. INEPT-enhanced signals may appear less intense in CP, and the opposite may also occur, see Fig. S1 (ESI†). This observation suggests the existence of distinct subpopulations of resonances in the sample, each with varying mobilities.[49]

Fig. 7(b) shows the CP spectra of *bchQ* (red) and WT (black) chlorosomes. The ^{13}C-5 signal at 102 ppm of the major fraction is better resolved for *bchQ* in comparison to WT chlorosomes. The CP signals for the rigid ^{13}C resonances resolved in the spectra are 13^1-C, 17^3-C, 14-C, 16-C, 1-C, 6-C, 9-C, 4-C, 3-C, 2-C, 10-C, 15-C, 5-CH, 3^1-CH, F1-CH$_2$, 17-CH, 18-CH, 17^1-CH$_2$, 17^2-CH$_2$, F8-CH$_2$, F5-CH$_2$, 3^2-CH$_3$, F3^1-CH$_3$, 2^1-CH$_2$, 7^1(II)-CH$_3$. The 20-C, 15-C, and 5-C(II) methine signals overlap with the 10-C signal. The signals located in the aliphatic region in the CP spectra are broad, which can be attributed to sample heterogeneity.

Fig. 7(c) presents an overlaid DP spectrum of *bchQ* (red) and WT (black) chlorosomes showing signals for all the ^{13}C resonances present in the sample irrespective of the mobility.

The signal for *bchQ* shows a significant increase in intensity around 60–80 ppm and 100 ppm. Strong signals are detected in these regions from the sugar headgroups of the galactolipids and the anomeric carbons at 100 ppm surrounding the chlorosomes.[15] The increase in relative intensity for these signals for chlorosomes from the *bchQ* mutant indicates that there may be an increase of the lipid to BChl ratio for *bchQ* compared to the WT, which would be in line with smaller chlorosomes in *bchQ* compared to WT observed with TEM.[23]

4. Discussion

By combining solid-state NMR, cryo-EM, and optical methods, we were able to retrieve information about chlorosomes of the *bchQ* mutant that is usually gathered separately from bacteria that may have been grown under varying conditions. Moreover, we made sure that we reproduced known results for the WT chlorosomes, a system that serves as a reference, using the same procedures. Solid-state NMR is a widely used technique for resolving structure and dynamics, for systems such as proteins, amyloids, supramolecular aggregates, polymers.[50–55] We employed the two-dimensional ^{13}C–^{13}C RFDR, dipolar hCH to get the ^{13}C and ^{1}H assignments. CHHC spectra were used to probe the distance constraints. It showed ^{1}H–^{1}H distances of less than 5 Å. This agrees well with the proton transfer range previously established for this experiment. The data reveals the presence of parallel stacking motifs, as seen also for the WT chlorosomes.

1D solid-state NMR experiments CP, INEPT, and DP were also applied to provide insight into the global dynamics properties. Recent progress on MAS NMR has demonstrated the importance of using both dipolar and *J*-based pulse sequences for probing rigid and dynamic components in the system and in turn elucidating the structure and dynamics of a system under study.[32,56] On a higher structural level, cryo-EM can be employed to obtain insight into molecular packing and supramolecular structuring.[26,27,57] As chlorosomes self-assemble into an array of stacks without incorporating proteins into the stacks, this makes chlorosomes a less complex system to study the relationship between structure and function compared to their protein-pigment-based counterparts. On the other hand, chlorosomes are intrinsically disordered systems, featuring both static and dynamic disorder,[28] and the fine structure of chlorosomes has long eluded our characterisation efforts. Comparing the composition of WT and *bchQ* chlorosomes, *i.e.*, the degree of static disorder, the WT chlorosome is considerably more heterogenous, with variable degrees of methylation at 8^2-C and 12^1-C, see Fig. S7 (ESI†). Yet, one may conclude from the ^{13}C–^{13}C RFDR and CHHC data that *bchQ* and WT chlorosomes both exhibit alternate parallel stacking of *syn–anti* monomers. On the other hand, the optical response measured for the two chlorosome types show remarkable differences. Because of the *syn–anti* parallel stacking, both are redshifted by 60–80 nm compared to monomeric BChl *c* in solution. The absorption spectra of *bchQ* showed a narrower and 15 nm blue
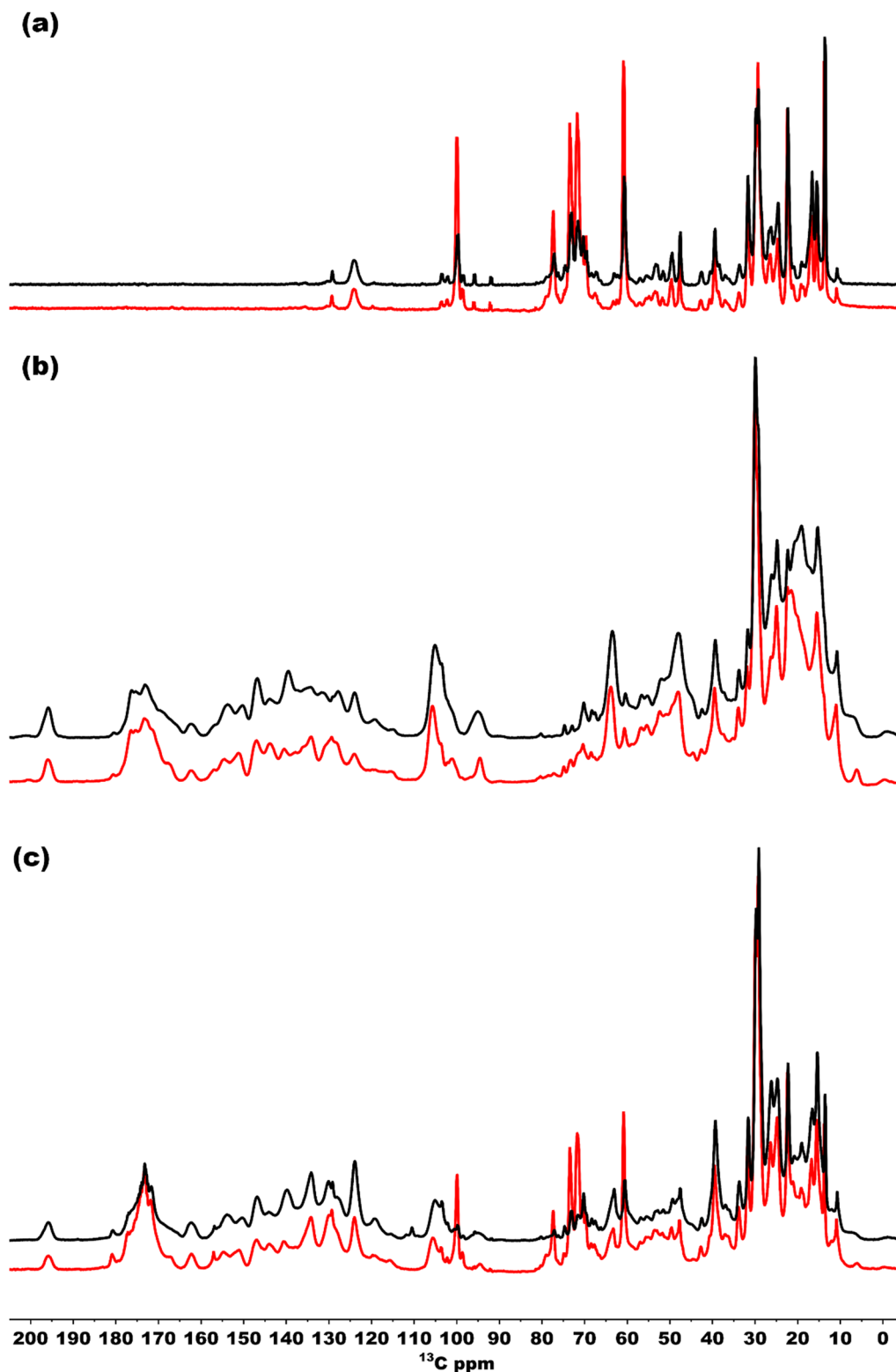
15862 | *Phys. Chem. Chem. Phys.*, 2024, **26**, 15856–15867

This journal is © the Owner Societies 2024

Fig. 7 (a)–(c) Overlaid INEPT, CP, and DP spectra of *bchQ* (red) and WT (black) chlorosomes, respectively, recorded in a 3.2 mm rotor spinning at 20 kHz at 277 K. The DP, CP and INEPT spectra were normalized at the highest intensity.

shifted Q_y band compared to WT. The 15-nm red-shift for WT chlorosomes compared to *bchQ* mutant chlorosomes suggests that WT has better potential for light harvesting because WT

has a larger window to utilize light in the far-red region that can be utilized for light harvesting.[23] The red shift of 15 nm in the absorption maximum for the WT in comparison to *bchQ*

chlorosomes can be attributed to several factors, including compositional differences between WT and *bchQ*, or total number of BChl molecules in the assembly, as discussed in the literature.[23] Also, chirality can provide a contribution. Model calculations show that a different overall chirality can shift the position of the absorption maximum by as much as 7 nm.[20] The red-shift is also reflected in the corresponding CD spectra. Apparently, an increased number of homologs, *e.g.*, for the WT, gives rise to the growth of larger chlorosomes.[13]

Because CD spectra are sensitive to supramolecular chirality, one may use this relation for determining chirality. The internal chirality of a molecule results in psi shaped bands in the CD spectra of large chiral aggregates.[58] For chlorosomes, four types of CD bands were reported: type 1, positive negative (+/−), type II, negative positive (−/+), and two mixed types, negative positive negative (−/+/−) and positive negative positive (+/−/+).[8] This signature also changes for tubes that are very short compared to the size of natural chlorosomes.[59] Previously, Li *et al.* developed a computational procedure that directly relates the signature of the CD signal to the chiral angle. It shows that each signature can be attributed to regions of chiral angles, albeit that domain boundaries are affected by spectral broadening.[24] Moreover, the CD signals undergo a sign inversion if the direction of rolling is switched, *i.e.*, when the inside and outside of a tube are interchanged. While the CD spectra of chlorosomes for WT and the *bchQ* mutant exhibit rather similar signatures, the details differ significantly. Combined with layer line information, the clear −/+/− bands for the WT narrow down the number of commensurate chiral angles to a few distinct values, including a chiral angle of 112, see Fig. S5 (ESI†).[20] On the other hand, the reduction of the compositional heterogeneity for *bchQ* chlorosomes relative to WT induces a change to a −/+ type pattern, since the negative band at *ca.* 720 strongly increases relative to WT, while the strong

negative band between 750–800 nm for WT virtually disappears for the *bchQ* chlorosomes with predominantly 95% [8Et, 12Et]-BChl *c*. This change in the signature reflects a change in the angle between the stacks and the tube axis for *bchQ* relative to WT. A chiral angle of 90° is both relatively close to the proposed values of 112° for WT and consistent with this signature.

Although in this study sample variability has been minimized *via* improved preparation protocols, other effects on the CD spectra collected from ensembles of chlorosomes, in particular a varying signal with length in the lower size range, has long been considered to seriously challenge the direct interpretation of optical information for ensembles of chlorosomes.[60,61] Moreover, calculations indicate that CD spectra for model chlorosomes become length-independent beyond 60 nm, which sets a more precise limit for this relation.[24] We note that measured dimensions for both WT and *bchQ* chlorosomes are greater than 90 nm according to TEM, thereby sufficiently exceeding this theoretical lower limit.[23]

As discussed, the observation of layer lines in the Fourier transform cryo-EM data of *bchQ* chlorosomes is crucial for their structural characterization, as it corroborates evidence for their helical nature. The layer line position in reciprocal space directly relates to the distance between subunits along the direction of the tube axis in real space.[62] A repeat of 1.25 nm was previously identified for WT, meaning that the repeat of 1.49 nm determined for *bchQ*, reflects a significant difference in BChl stacking (Fig. 8).

Using a geometrical analysis developed by Li *et al.*[20,24] This measured layer line position for the *bchQ* mutant relates to chiral angles $\delta = 57°, 89°, 90°, 123°, 160°, 172°$ depending on the chiral family that one considers, see Fig. S6 (ESI†), with the direction of rolling making no difference. Among these, only four angles, namely $\delta = 57°, 90°, 123°$ and $160°$, also match the signature of the CD spectra. We note that $\delta = 90°$ gives rise to
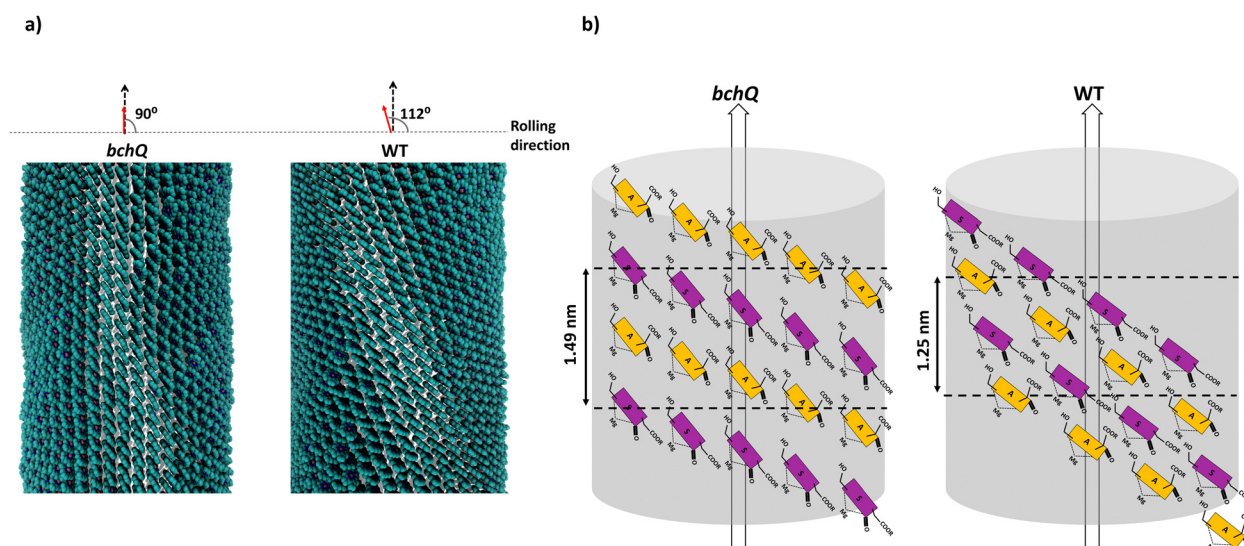
a)

b)

Fig. 8 (a) Shows the atomistic tube model for *bchQ* chlorosomes obtained by combining MAS NMR, cryo-EM and CD measurements, and (b) shows the schematic representation of the *syn−anti* stacking in the tubes. Both the atomistic model and the *syn−anti* stacking framework are compared with WT to highlight the structural differences.

15864 | *Phys. Chem. Chem. Phys.*, 2024, **26**, 15856–15867

This journal is © the Owner Societies 2024

the previously proposed stacking mode parallel to the tube axis.[26,27] It is important to note that although CD lacks the precision to resolve pigment arrangements, it does provide information about the interaction of electronic transition dipoles within pigments. Small changes may lead to a shift of absorption maximum and alter the position of the negative and positive CD bands.[25,46] Combining data from different characterization methods, *i.e.* CD and cryo-EM, enables us to narrow down commensurate chiral angles, using the protocol outlined by Li *et al.*[20,24] To compare beyond the feature of the layer line, we performed Fourier analysis on an atomically resolved chlorosome model for the commensurate chiral angles associated with the reverse rolling direction, which is the one associated with $\delta = 112°$ proposed for the WT chlorosomes. Direct comparison of simulated scattering features indeed shows distinct similarities for $\delta = 90°$ (Fig. 5c and d), while matching to the other angles $57°$, $123°$, $160°$ is difficult. Since the CD signals for $\delta = 90°$ (*bchQ*) and $\delta = 112°$ (WT) are both from the helical H(0,1) family, it is tempting to conclude that the two distinct chiral angles explain the available information for the two chlorosome types. The small shoulder around 750–800 in the CD spectrum for the *bchQ* chlorosomes is then due to the remaining 5% methylation at C12 and heterogeneity within the system, including distributions in tube lengths. The role of overall chirality of the BChl stacks on the particulars of exciton transfer was recently evaluated computationally.[25]

A global perspective on the dynamics was obtained by performing one-dimensional NMR spectroscopy. For the spectra acquired using direct polarization, the differences between *bchQ* and WT chlorosomes are primarily in the region between 65–80 ppm, which corresponds to galactosyl lipid groups present in the system. It appears that *bchQ* contains a larger amount of lipids than WT. This is due to the fact that chlorosomes are smaller in size as shown by Gomez Maqueo Chew *et al.* using Transmission Electron Microscopy (TEM) images.[23] This smaller size in chlorosomes leads to increased lipid to BChl ratio in *bchQ* compared to WT.[63]

Most of the NMR signals of BChl *c* appear in the CP-based spectrum for both WT and *bchQ* chlorosomes. However, the signals for chlorosomes from the *bchQ* mutant are better resolved compared to WT. This confirms that the BChl *c* aggregates in chlorosomes from the *bchQ* mutant are more ordered and homogenous because of less methylation and the presence of a single homolog.[23] The INEPT works like a solution state experiment which gives signals if there is through bond coupling and probes flexible regions in the system. The INEPT spectra show a major increase in signal intensity of the *bchQ* chlorosomes for the lipid region and the fact that both WT and *bchQ* chlorosomes samples show signals in INEPT around that region, points simply to increased lipids to BChl ratio present in chlorosomes of the *bchQ* mutant. The other signals observed in INEPT, which belong to side groups and tails, show similar dynamic trends. Overall, we may conclude that chlorosomes of the *bchQ* mutant and WT display equivalent dynamical properties. This suggests the idea that chlorosomes can be considered as plastic crystals. In this model, the

rigid macrocycle core is crystalline while the tails attached to it are dynamic. However, a property that characterizes plastic crystals – rotational mode – has not yet been observed. This is because any distinguishing dynamics related to pigment rotation would be too fast for our current NMR setup to detect.[20]

5. Conclusions

By modifying the BChl biosynthetic pathway, a mutant chlorosome with reduced compositional and structural heterogeneity compared to WT has been produced.[23] The *bchQ* mutant, containing 95% [8Et, 12Et], closely matches the entirely homogeneous setup in existing molecular dynamics (MD) simulations, setting the stage for a more thorough understanding of the structure–function properties of chlorosomes through MAS NMR, cryo-EM, and optical data. Proton and carbon chemical shift assignments have been obtained using 2D RFDR and dipolar hCH experiments. Distance constraints obtained from CHHC spectra showed the same alternate parallel stacking of *syn–anti* monomers in *bchQ* as obtained earlier for WT chlorosomes. cryo-EM data revealed the characteristic tube chirality of chlorosomes, but with an axial repeat of 1.49 nm and a separation of 2.1 nm between tubes. Optical data was also obtained for chlorosomes from the *bchQ* mutant. Apart from showing that the absorption and CD spectra are substantially different from the WT spectra, in combination with cryo-EM data they provide us the means for further narrowing down matching chiral angles for *bchQ*.

Our measurements reveal differences between *bchQ* and WT chlorosomes. On the smallest molecular scale, the unit cell containing a *syn–anti* dimer is conserved between the WT and the *bchQ* mutant. The modification of the composition upon mutation with limited side chain heterogeneity leads to a blue-shifted absorption maximum for the *bchQ* chlorosomes, and a significantly different layer line position and CD spectra type. The increased molecular homogeneity results in better resolved half-bandwidth in the absorption spectra, which may explain the need for homolog heterogeneity in WT chlorosomes.

The protocol developed in this study is applicable to artificial systems with tubes or multistart helices, to extract the overall chirality of the assemblies formed by synthetic molecules. The *syn–anti* parallel stacking of BChl in chlorosomes[26,27] is known to be different from the stacking in most artificial analogues, in which the farnesyl chain is replaced.[64] Molecular modifications will most often lead to antiparallel packing.[65] Very recently also parallel stacked analogs have been presented, albeit that bulky side chains instead of farnesyl chain change the overall morphology.[64] It can be noted, however, that for parallel stacks and sheets, chirality does not necessarily translate into functional information, as exemplified by the conservation of function for different chiralities in chlorosomes.

The main purpose of our study is to resolve a structure for the primary homolog that was consistently used in modelling

This journal is © the Owner Societies 2024

Phys. Chem. Chem. Phys., 2024, **26**, 15856–15867 | **15865**

studies, tacitly assuming there would be no difference between a mixture of homologs and a pure single ethyl–ethyl homolog. The further we progress in drawing conclusions from the modelling, the more urgent it is to have a structural basis as close as possible to the models. The present study fulfills that need. The main outcomes of this study, which also support earlier findings, indicate that the differences between *bchQ* and WT are small (Fig. 8). Earlier results indicate that the effects of differences in chirality on exciton transfer are minor.[25] Hence the specific chirality is not critical for the function.

With MAS NMR, it has been observed that chlorosomes exhibit significant dynamics despite the presence of large supramolecular aggregates. We observed dynamics in the side chain and tail carbon resonances, which provided a comprehensive view of the NMR time scale dynamics. Our data are in line with the plastic crystalline character proposed by Li *et al.*[20] Which supports the idea that the macrocycle core is crystalline but there is a fast rotational motion in the ps time scale which couples to the exciton energy levels, promoting long-range energy transfer by modulating energy levels and overlap between exciton states. This spectral information is influenced by local fluctuations and should be further investigated in the future.

Conflicts of interest

There are no conflicts to declare.

Acknowledgements

Notes and references

1 T. M. Wahlund, C. R. Woese, R. W. Castenholz and M. T. Madigan, *Arch. Microbiol.*, 1991, **156**, 81–90.

2 J. T. Beatty, J. Overmann, M. T. Lince, A. K. Manske, A. S. Lang, R. E. Blankenship, C. L. Van Dover, T. A. Martinson and F. G. Plumley, *Proc. Natl. Acad. Sci. U. S. A.*, 2005, **102**, 9306–9310.

3 L. Andrew Staehelin, J. R. Golecki and G. Drews, *Biochim. Biophys. Acta, Bioenerg.*, 1980, **589**, 30–45.

4 J. Dostal and D. Zigmantas, *J. Am. Chem. Soc.*, 2012, 7.

5 G. T. Oostergetel, H. van Amerongen and E. J. Boekema, *Photosynth. Res.*, 2010, **104**, 245–255.

6 C. M. Borrego and L. J. Garcia-Gil, *Photosynth. Res.*, 1995, **45**, 21–30.

7 C. M. Borrego, P. D. Gerola, M. Miller and R. P. Cox, *Photosynth. Res.*, 1999, **59**, 159–166.

8 A. R. Holzwarth, K. Griebenow and K. Schaffner, *J. Photochem. Photobiol. Chem.*, 1992, **65**, 61–71.

9 J. Dostál, J. Pšenčík and D. Zigmantas, *Nat. Chem.*, 2016, **8**, 705–710.

10 N. C. M. Magdaong, D. M. Niedzwiedzki, R. G. Saer, C. Goodson and R. E. Blankenship, *Biochim. Biophys. Acta, Bioenerg.*, 2018, **1859**, 1180–1190.

11 S. K. Frehan, L. Dsouza, X. Li, V. Eríc, T. L. C. Jansen, G. Mul, A. R. Holzwarth, F. Buda, G. J. A. Sevink, H. J. M. de Groot and A. Huijser, *J. Phys. Chem. B*, 2023, **127**, 7581–7589.

12 N.-U. Frigaard and D. A. Bryant, in *Complex Intracellular Structures in Prokaryotes*, ed. J. M. Shively, Springer Berlin Heidelberg, Berlin, Heidelberg, 2006, vol. 2, pp. 79–114.

13 N.-U. Frigaard and D. A. Bryant, *Arch. Microbiol.*, 2004, **182**, 265–276.

14 B.-J. van Rossum, D. B. Steensgaard, F. M. Mulder, G. J. Boender, K. Schaffner, A. R. Holzwarth and H. J. M. de Groot, *Biochemistry*, 2001, **40**, 1587–1595.

15 T. S. Balaban, A. R. Holzwarth, K. Schaffner, G.-J. Boender and H. J. M. de Groot, *Biochemistry*, 1995, **34**, 15259–15266.

16 X. Li, F. Buda, H. J. M. de Groot and G. J. A. Sevink, *J. Phys. Chem. C*, 2018, **122**, 14877–14888.

17 V. Erić, X. Li, L. Dsouza, S. K. Frehan, A. Huijser, A. R. Holzwarth, F. Buda, G. J. A. Sevink, H. J. M. de Groot and T. L. C. Jansen, *J. Phys. Chem. B*, 2023, **127**, 1097–1109.

18 J. Pšenčík, T. Polívka, P. Němec, J. Dian, J. Kudrna, P. Malý and J. Hála, *J. Phys. Chem. A*, 1998, **102**, 4392–4398.

19 G. A. Montaño, B. P. Bowen, J. T. LaBelle, N. W. Woodbury, V. B. Pizziconi and R. E. Blankenship, *Biophys. J.*, 2003, **85**, 2560–2565.

20 X. Li, F. Buda, H. J. M. De Groot and G. J. A. Sevink, *iScience*, 2022, **25**, 103618.

21 A. Pandit, K. Ocakoglu, F. Buda, T. van Marle, A. R. Holzwarth and H. J. M. de Groot, *J. Phys. Chem. B*, 2013, **117**, 11292–11298.

22 J. L. Thweatt, D. P. Canniffe and D. A. Bryant, *Adv. Bot. Res.*, 2019, **90**, 35–89.

23 A. G. M. Chew, N.-U. Frigaard and D. A. Bryant, *J. Bacteriol.*, 2007, **189**, 6176–6184.

24 X. Li, F. Buda, H. J. M. de Groot and G. J. Agur Sevink, *J. Phys. Chem. C*, 2019, **123**, 16462–16478.

25 V. Erić, J. L. Castro, X. Li, L. Dsouza, S. K. Frehan, A. Huijser, A. R. Holzwarth, F. Buda, G. J. A. Sevink, H. J. M. de Groot and T. L. C. Jansen, *J. Phys. Chem. B*, 2023, **127**, 7487–7496.

26 S. Ganapathy, G. T. Oostergetel, P. K. Wawrzyniak, M. Reus, A. Gomez Maqueo Chew, F. Buda, E. J. Boekema, D. A. Bryant, A. R. Holzwarth and H. J. M. de Groot, *Proc. Natl. Acad. Sci. U.S.A.*, 2009, **106**, 8525–8530.

15866 | *Phys. Chem. Chem. Phys.*, 2024, **26**, 15856–15867

This journal is © the Owner Societies 2024

27 S. Ganapathy, G. T. Oostergetel, M. Reus, Y. Tsukatani, A. Gomez Maqueo Chew, F. Buda, D. A. Bryant, A. R. Holzwarth and H. J. M. de Groot, *Biochemistry*, 2012, **51**, 4488–4498.

28 L. M. Günther, M. Jendrny, E. A. Bloemsma, M. Tank, G. T. Oostergetel, D. A. Bryant, J. Knoester and J. Köhler, *J. Phys. Chem. B*, 2016, **120**, 5367–5376.

29 L. M. Günther, A. Löhner, C. Reiher, T. Kunsel, T. L. C. Jansen, M. Tank, D. A. Bryant, J. Knoester and J. Köhler, *J. Phys. Chem. B*, 2018, **122**, 6712–6723.

30 Y. Tian, R. Camacho, D. Thomsson, M. Reus, A. R. Holzwarth and I. G. Scheblykin, *J. Am. Chem. Soc.*, 2011, **133**, 17192–17199.

31 G. S. Harbison and J. Herzfeld, *Biochemistry*, 1983, **22**, 1–5.

32 I. Matlahov and P. C. A. van der Wel, *Methods*, 2018, **148**, 123–135.

33 A. E. Bennett, R. G. Griffin, J. H. Ok and S. Vega, *J. Chem. Phys.*, 1992, **96**, 8624–8627.

34 A. Lange, S. Luca and M. Baldus, *J. Am. Chem. Soc.*, 2002, **124**, 9704–9705.

35 I. De Boer, L. Bosman, J. Raap, H. Oschkinat and H. J. M. De Groot, *J. Magn. Reson.*, 2002, **157**, 286–291.

36 K. R. Thurber and R. Tycko, *J. Magn. Reson.*, 2009, **196**, 84–87.

37 E. K. Paulson, C. R. Morcombe, V. Gaponenko, B. Dancheck, R. A. Byrd and K. W. Zilm, *J. Am. Chem. Soc.*, 2003, **125**, 14222–14223.

38 E. Barbet-Massin, A. J. Pell, J. S. Retel, L. B. Andreas, K. Jaudzems, W. T. Franks, A. J. Nieuwkoop, M. Hiller, V. Higman, P. Guerry, A. Bertarello, M. J. Knight, M. Felletti, T. Le Marchand, S. Kotelovica, I. Akopjana, K. Tars, M. Stoppini, V. Bellotti, M. Bolognesi, S. Ricagno, J. J. Chou, R. G. Griffin, H. Oschkinat, A. Lesage, L. Emsley, T. Herrmann and G. Pintacuda, *J. Am. Chem. Soc.*, 2014, **136**, 12489–12497.

39 M. Weingarth, P. Tekely and G. Bodenhausen, *Chem. Phys. Lett.*, 2008, **466**, 247–251.

40 D. H. Zhou and C. M. Rienstra, *J. Magn. Reson.*, 2008, **192**, 167–172.

41 J. Schindelin, I. Arganda-Carreras, E. Frise, V. Kaynig, M. Longair, T. Pietzsch, S. Preibisch, C. Rueden, S. Saalfeld, B. Schmid, J.-Y. Tinevez, D. J. White, V. Hartenstein, K. Eliceiri, P. Tomancak and A. Cardona, *Nat. Methods*, 2012, **9**, 676–682.

42 R. J. Abraham and K. M. Smith, *J. Am. Chem. Soc.*, 1983, **105**, 5734–5741.

43 C. M. Quinn, M. Wang and T. Polenova, in *Protein NMR*, ed. R. Ghose, Springer New York, New York, NY, 2018, vol. 1688, pp. 1–35.

44 J. Knoester, *Int. J. Photoenergy*, 2006, 1–10.

45 G. Garab and H. van Amerongen, *Photosynth. Res.*, 2009, **101**, 135–146.

46 D. C. Brune, P. D. Gerola and J. M. Olson, *Photosynth. Res.*, 1990, **24**, 253–263.

47 F. Azadi-Chegeni, C. Schiphorst and A. Pandit, *Photosynth. Res.*, 2018, **135**, 227–237.

48 F. Azadi Chegeni, G. Perin, K. B. Sai Sankar Gupta, D. Simionato, T. Morosinotto and A. Pandit, *Biochim. Biophys. Acta, Bioenerg.*, 2016, **1857**, 1849–1859.

49 H.-K. Lin, J. C. Boatz, I. E. Krabbendam, R. Kodali, Z. Hou, R. Wetzel, A. M. Dolga, M. A. Poirier and P. C. A. van der Wel, *Nat. Commun.*, 2017, **8**, 15462.

50 M. Weingarth and M. Baldus, *Acc. Chem. Res.*, 2013, **46**, 2037–2046.

51 P. C. A. van der Wel, *Emerg. Top. Life Sci.*, 2018, **2**, 57–67.

52 B. Reif, S. E. Ashbrook, L. Emsley and M. Hong, *Nat. Rev. Methods Primers*, 2021, **1**, 2.

53 P. Schanda and M. Ernst, *Prog. Nucl. Magn. Reson. Spectrosc.*, 2016, **96**, 1–46.

54 F. Castellani, B. van Rossum, A. Diehl, M. Schubert, K. Rehbein and H. Oschkinat, *Nature*, 2002, **420**, 99–102.

55 A. Abragam, *The Principles of Nuclear Magnetism*, Clarendon Press, 1983.

56 O. C. Andronesi, S. Becker, K. Seidel, H. Heise, H. S. Young and M. Baldus, *J. Am. Chem. Soc.*, 2005, **127**, 12965–12974.

57 A. Alia, F. Buda, H. J. M. de Groot and J. Matysik, *Annu. Rev. Biophys.*, 2013, **42**, 675–699.

58 Y. Miloslavina, P. H. Lambrev, T. Jávorfi, Z. Várkonyi, V. Karlický, J. S. Wall, G. Hind and G. Garab, *Photosynth. Res.*, 2012, **111**, 29–39.

59 C. Didraga, J. A. Klugkist and J. Knoester, *J. Phys. Chem. B*, 2002, **106**, 11474–11486.

60 C. Didraga and J. Knoester, *J. Lumin.*, 2003, **102–103**, 60–66.

61 T. Kunsel, L. M. Günther, J. Köhler, T. L. C. Jansen and J. Knoester, *J. Chem. Phys.*, 2021, **155**, 124310.

62 G. T. Oostergetel, M. Reus, A. Gomez Maqueo Chew, D. A. Bryant, E. J. Boekema and A. R. Holzwarth, *FEBS Lett.*, 2007, **581**, 5435–5439.

63 Y. Tsukatani, J. Harada, T. Mizoguchi and H. Tamiaki, *Photochem. Photobiol. Sci.*, 2013, **12**, 2195.

64 A. Löhner, T. Kunsel, M. I. S. Röhr, T. L. C. Jansen, S. Sengupta, F. Würthner, J. Knoester and J. Köhler, *J. Phys. Chem. Lett.*, 2019, **10**, 2715–2724.

65 S. Ganapathy, S. Sengupta, P. K. Wawrzyniak, V. Huber, F. Buda, U. Baumeister, F. Würthner and H. J. M. de Groot, *Proc. Natl. Acad. Sci. U. S. A.*, 2009, **106**, 11472–11477.

This journal is © the Owner Societies 2024

Phys. Chem. Chem. Phys., 2024, **26**, 15856–15867 | **15867**